ChemComm

Elimination of homogeneous broadening in 1H solid-state NMR

Journal:	*ChemComm*
Manuscript ID	CC-COM-05-2024-002191.R1
Article Type:	Communication

ChemComm

COMMUNICATION

DOI: 10.1039/x0xx00000x

Elimination of homogeneous broadening in ^{1}H solid-state NMR

Received 00th January 20xx,
Accepted 00th January 20xx

Frédéric A. Perras,*[a,b]

^{1}H solid-state NMR spectra are plagued by low resolution, necessitating the use of complex pulse sequences or specialized equipment. We introduce a new resolution enhancement method, inspired by super-resolution microscopy, that uses a 2D Hahn-echo experiment to constrain deconvolution. The result is an effective doubling of the MAS frequency.

^{1}H solid-state nuclear magnetic resonance (NMR) spectroscopy is plagued by poor resolution that stems from the non-refocusable homonuclear dipolar interactions between neighboring ^{1}H spins. As such, despite the ubiquity of solution-phase ^{1}H NMR, studies of solid materials have never been routine. From 1965 to 2000, the leading strategy for acquiring high-resolution ^{1}H NMR spectra were the cantankerous combined rotation and multiple-pulse sequences (CRAMPS) which combined slow magic-angle spinning (MAS) with homonuclear dipolar recoupling.[1-9] In 2000, however, Samoson and Varian developed MAS probes capable of reaching rotation frequencies (ν_R) of 50 kHz,[10,11] greater than typical ^{1}H homonuclear dipolar interactions (c.a. 20 kHz), providing useful resolution without needing complicated pulse sequences, enabling indirect detection via protons.[12-17] Resolution can also be further increased by leveraging the higher chemical shift dispersion in 2D and 3D multiple-quantum experiments.[18] Further advances in spinning technology have continued to increase the accessible MAS frequencies to 170 kHz via rotor miniaturization.[19-21]

Fast-MAS ^{1}H NMR spectra are unfortunately never isotropic.[22-24] The homogeneous homonuclear dipolar broadening is reduced at a rate of $1/\nu_R$ as MAS frequencies are increased, implying that infinite MAS rates would be required to maximize resolution. In practice, recent estimates suggest that spinning frequencies of 300 kHz may be sufficient to reach optimal resolution in biomolecular systems;[25] higher frequencies may be necessary for rigid solids. Non-refocusable decay can be eliminated using a constant-time CRAMPS or fast-MAS experiment, but resolution is nevertheless limited by the coherence lifetimes.[26-28] As such, a third strategy to achieve high-resolution ^{1}H solid-state NMR spectra has been proposed by Emsley *et al*.[29] that borrows many core concepts from resolution-enhanced microscopy.[30-33] Specifically, if information can be gained about the homogeneous linewidth of the resonances, then deconvolution can be applied to extract the pure isotropic ^{1}H MAS spectrum. Similar ideas have also been applied for *J* decoupling.[34] Emsley *et al.* have achieved this by monitoring the ν_R-dependence of the linewidths and, more recently, via machine learning.[35] The former method can be summarized by the following. The NMR spectrum is expressed as a column vector, **S**, with TD equally-spaced points. Each point, i, has its own intensity (I_i) and linewidth, which is assumed to be inversely-dependent on the MAS frequency (σ_i/ν_R, where σ_i is a MAS-independent linewidth coefficient). The final spectrum is a convolution of these intensities with their characteristic linewidths.

$$\mathbf{S} = \mathbf{G} \cdot \mathbf{I} \quad (1)$$

The rows of the lineshape matrix, **G**, can be expressed as Gaussian functions, but can in principle take any form.

$$G_i(\nu,\nu_R,\sigma_i) = \frac{\nu_R}{\sigma_i\sqrt{2\pi}}\exp\left(-\frac{\nu_R^2}{2}\left(\frac{\nu_i-\nu}{\sigma_i}\right)^2\right) \quad (2)$$

Spectra acquired at a variety of ν_R values can be simultaneously fitted to determine the vector of MAS-independent linewidth coefficients, **σ**, and the vector of isotropic intensities, **I**.

$$\min_{\mathbf{I},\boldsymbol{\sigma}} \sum_{\nu_{R,min}}^{\nu_{R,max}} \|\mathbf{S}(\nu_R) - \mathbf{G}(\nu_R)\cdot\mathbf{I}\| \quad (3)$$

Herein we build on this foundation by noting that the convolution functions, **G**(ν_R), can be measured independently by performing a 2D Hahn-echo experiment.[36] Experimental knowledge of **σ** halves the number of independent values to be determined by deconvolution, and the reliability of pure isotropic spectrum reconstruction.

The general procedure for this Hanh-echo assisted deconvolution (HEAD) experiment is outlined in **Figure 1**. First a 2D Hahn-echo experiment is performed with the same digital resolution in both spectral dimensions. The cosine transformation of this dataset along t_1 produces a spectrum that correlates the convoluted NMR spectrum, **S**, to the scaled homogeneous lineshapes at each frequency, **G'**=**S**∘**G**. Note that ∘ indicates a Hadamard product. In practice the cosine transformation is done by inserting free induction decays of zero intensity in between each t_1 increment and then the spectrum is processed using the States method (see pulse

[a] Chemical and Biological Sciences Division, Ames National Laboratory, Ames, IA 50011
[b] Department of Chemistry, Iowa State University, Ames, IA 50011

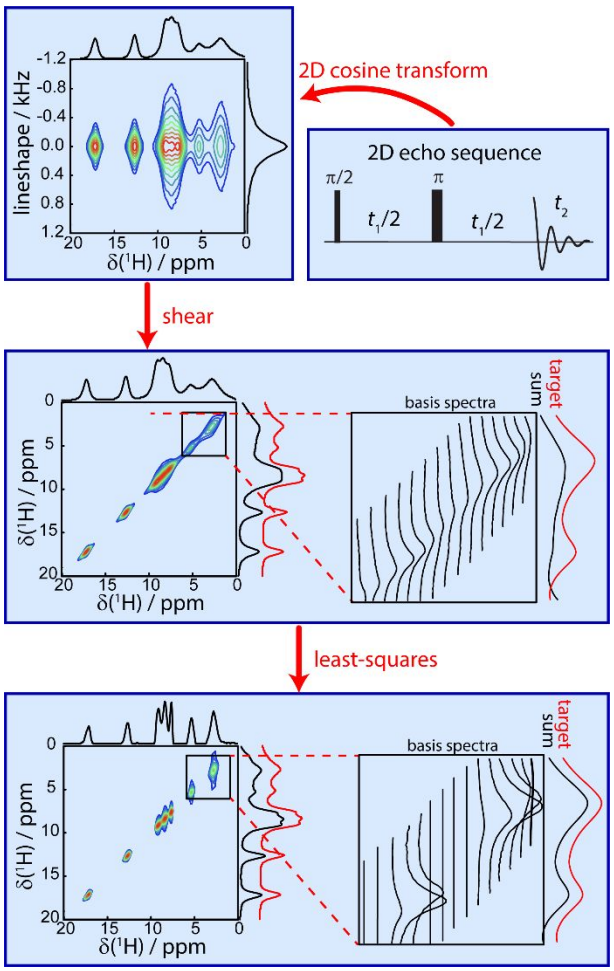

Figure 1. Graphical depiction of the HEAD process. Starting from the 2D cosine transform of a Hahn-echo experiment (**S** vs. **G'**), a shearing transform is applied to generate individual basis spectra in F1 containing the characteristic linewidth of the resonance at that frequency (**S** vs. **G'·S**). Integrating over these columns produces a convoluted spectrum with broader lineshapes than that seen in F2 (red). A least-squares refinement is then performed over the intensities in F2 to minimize the difference between the sum projection in F1 and the original sum projection along F1 (**I** vs. **S**). The result is a reduction in linewidths due to deconvolution.

program). [37] The spectrum is then sheared to produce a spectrum correlating **S** to **G'·S**. Note that this convoluted spectrum would equal the MAS spectrum in the event that the homogeneous broadening was negligible: i.e **S**= **I**.

We then perform a least-squares refinement to produce a spectrum correlating **S**∘**W**, where the vector **W** contains weights applied to the experimental spectrum **S**, to a prediction of the experimental **S**≈**G'**·(**S**∘**W**). The weights are minimized as follows using a Broyden–Fletcher–Goldfarb–Shanno (BFGS) algorithm.

$$\min_{\mathbf{W}} \|\mathbf{S} - \mathbf{G}' \cdot (\mathbf{S} \circ \mathbf{W})\| \quad (4)$$

The initial values of the **W** vector are set to 1. The least-squares optimization is stabilized with the use of Tikhonov regularization, where the weighting parameter λ is chosen to balance the noise and resolution of the produced spectrum. The optimal value for λ is selected by manual inspection, but we have found good success with values on the order of 0.001.

$$\min_{\mathbf{W}} \|\mathbf{S} - \mathbf{G}' \cdot (\mathbf{S} \circ \mathbf{W})\| + \lambda \|L\mathbf{W}\| \quad (5)$$

In equation 5, the $\|L\mathbf{W}\|$ is calculated as

$$\|L\mathbf{W}\| = \sqrt{\sum_{\mathbf{i=1}}^{\mathbf{TD}} (W_i - W_{i-1})^2} \quad (6)$$

where W_i is the weight for the ith basis spectrum. Note that this procedure is conceptually similar to employing knowledge of the point spread function in microscopy to perform image deconvolution.[30-33] The approximation to the pure isotropic spectrum, **I**, is obtained by integrating this spectrum over **G'**. Note that $\mathbf{1}_{TD}$ is a vector of TD elements, all of which being equal to 1.

$$\mathbf{I} \approx (\mathbf{G}' \cdot \mathbf{1}_{TD}) \circ (\mathbf{S} \circ \mathbf{W}) \quad (7)$$

It is important to note that this procedure makes no assumptions on the form of the data (number of peaks, linewidths, etc.) and simply performs a direct fitting of the 1D spectrum against the experimental basis spectra obtained from the vertical slices sheared 2D echo spectrum (**Figure 1**, right).

The reliability of this approach was first tested using synthetic HEAD 2D spectra. The spectra consisted of three equally-spaced resonances, at 4, 5, and 6 ppm, with variable levels of line broadening or signal-to-noise. The results of the HEAD processing on these spectra are shown in **Figure 2**. Generally, we see that the resolution is degraded when the signal-to-noise ratio falls below 32, but the linewidths and positions are otherwise consistent for lower noise levels. Because ^{1}H's have a high NMR receptivity, noise is not expected to be a problem.

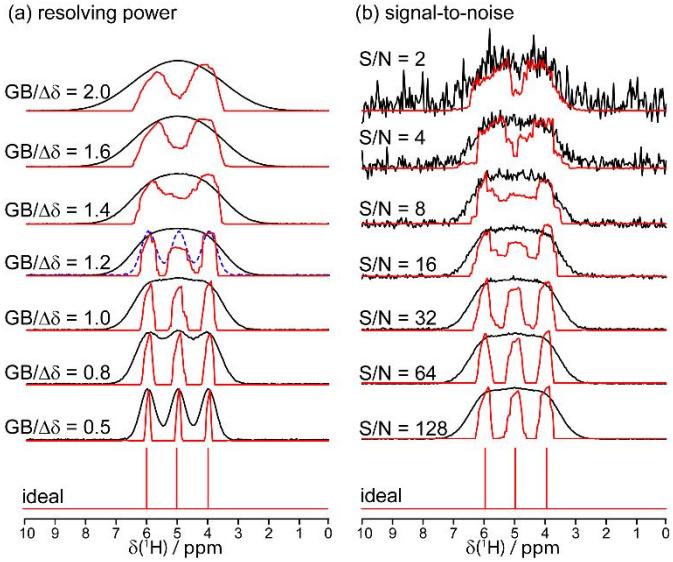

Figure 2. HEAD resolution enhancement trials using an idealized spectrum, shown on the bottom, and different levels of Gaussian broadening (GB, a) and signal-to-noise ratios (b). The source spectra are shown in black, while the HEAD reconstructions are in red. In (a) the source spectrum with GB/Δδ=0.5 is compared to the HEAD spectrum with GB/Δδ=1.2 (dashed blue) to highlight the approximate 2.5-fold increase in resolution. In (a) the signal-to-noise ration is maintained at 64 while in (b) the GB/Δδ ratio is maintained at 1.0.

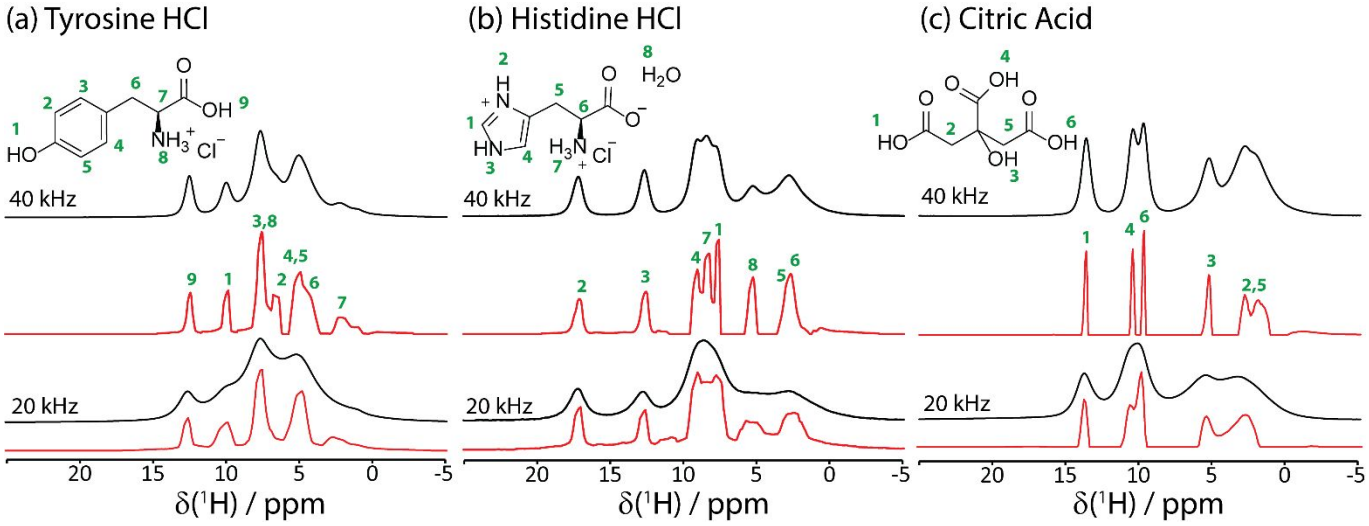

Figure 3. ^{1}H MAS (black) and HEAD isotropic reconstructions (red) measured for (a) tyrosine HCl, (b) histidine HCl, and (c) citric acid at MAS rates of 20 and 40 kHz, as indicated on the spectra. Compounds were purchases from Aldrich and used as received. Assignments are taken from prior literature.[29,38] Spectra were acquired on a Bruker AVANCE III 600 spectrometer equipped with a 1.6 mm Varian MAS probe. 8 scans were acquired for each of the 64 t_1 increments with the ^{1}H radiofrequency power set to 100 kHz. Increments were of 800 and 400 µs for the spectra acquired at 40 and 20 kHz, respectively. Recycle delays were set to 4 s with the exception of citric acid where this was increased to 200 s. The pulse program is available in a GitHub repository, together with the program used to process the spectra.[37]

As we varied the linewidths at half height from 0.5 ppm to 2.0 ppm, while maintaining the signal-to-noise ratio at 64, we see a progressive loss in resolution. When the linewidth exceeds the peak spacing by 40%, we can no longer discern the middle peak. The HEAD isotropic spectrum obtained with GB/$\Delta\delta$ = 1.2 was similar to the spectrum with GB/$\Delta\delta$ = 0.5. This suggests that we can expect roughly 2.5-fold improvement in resolution from HEAD when homogeneous broadening is dominant. This level of resolution enhancement is in line with that which is achievable from deconvolution in microscopy and likely represents a fundamental limitation of this form of deconvolution.[39-41]

We tested the performance of HEAD experimentally using tyrosine hydrochloride, histidine hydrochloride, and citric acid at MAS frequencies of 20 and 40 kHz. The standard 1D spectra and their HEAD resolution-enhanced spectra are shown in **Figure 3** in black and red, respectively. The experimental results corroborate those obtained from the synthetic spectra in that resolution is effectively doubled after deconvolution. The HEAD spectra acquired at 20 kHz MAS rate have comparable linewidth and resolution to those acquired at 40 kHz, while the HEAD spectra acquired at 40 kHz have spectacular resolution, similar to what is typically obtained at MAS rates near 100 kHz.[29,42,43] Importantly, these experiments demonstrate that HEAD can resolve occluded peaks, such as the three resonances near 8 ppm in histidine which appear as a single Gaussian peak at 20 kHz and are nevertheless discernible using HEAD.

To summarize, we have shown that 2D Hahn-echo experiments can be used to independently measure the frequency-dependent ^{1}H MAS NMR lineshapes, which can in turn be used for resolution enhancement via constrained deconvolution. This builds on the approach introduced by Moutzouri *et al.*,[29] by removing all assumptions regarding the form of lineshapes and their behavior with respect to the MAS frequency. The resulting process most closely mirrors the use of the point spread function in microscopy for resolution enhancement and similarly yields a 2-3-fold improvement in resolution, revealing otherwise occluded resonances. The resulting spectra are equivalent to a rough doubling of the MAS frequency.

Prof. Emily A. Smith is thanked for useful discussions. This work was supported by the U.S. Department of Energy (DOE), Office of Basic Energy Sciences, Division of Chemical Sciences, Geosciences, and Biosciences through a DOE Early Career Project. Ames National Laboratory is operated for the DOE by Iowa State University under Contract No. DE-AC02-07CH11358.

Conflicts of interest

There are no conflicts to declare.

Notes and references

1 M. Lee and I. Goldburg, *Phys. Rev. A* 1965, **140**, 1261.
2 J. S. Waugh, L. M. Huber and U. Haeberlen, *Phys. Rev. Lett.* 1968, **20**, 180.
3 W.-K. Rhim, D. D. Elleman and R. W. Vaughan, *J. Chem. Phys.* 1973, **59**, 3740.
4 B. C. Gerstein, R. G. Pembleton, R. C. Wilson and L. M. Ryan, *J. Phys. Chem. Lett.* 1977, **66**, 361.
5 M. H. Levitt, A. C. Kolbert, A. Bielecki and D. J. Ruben, *Solid State*

Nucl. Magn. Reson. 1993, **2**, 151.
6 M. Hohwy and N. C. Nielsen, *J. Chem. Phys.* 1997, **106**, 7571.
7 M. Hohwy, P. V. Bower, H. J. Jakobsen and N. C. Nielsen, *Chem. Phys. Lett.* 1997, **273**, 297.
8 D. Sakellariou, A. Lesage, P. Hodgkinson and L. Emsley, *Chem. Phys. Lett.* 2000, **319**, 253.
9 E. Vinogradov, P. K. Madhu and S. Vega, *Chem. Phys. Lett.* 1999, **314**, 443.
10 A. Samoson, T. Tuherm and Z. Gan *Solid State Nucl. Magn. Reson.* 2001, **20**, 130.
11 Y. Nishiyama, G. Hou, V. Agarwal, Y. Su and A. Ramamoorthy, *Chem. Rev.* 2023, **123**, 918.
12 Y. Ishii and R. Tycko, *J. Magn. Reson.* 2000, **142**, 199.
13 Y. Ishii, J. P. Yesinowski and R. Tycko, *J. Am. Chem. Soc.* 2001, **123**, 2921.
14 J. W. Wiench, C. E. Bronnimann, V. S.-Y. Lin and M. Pruski, *J. Am. Chem. Soc.* 2007, **129**, 12076.
15 K. Mao, J. W. Wiench, V. S.-Y. Lin and M. Pruski, *J. Magn. Reson.* 2009, **196**, 92.
16 A. Marchetti, S. Jehle, M. Felletti, M. J. Knight, Y. Wang, Z.-Q. Xu, A. Y. Park, G. Otting, A. Lesage, L. Emsley, N. E. Dixon, G. Pintacuda, *Angew. Chem. Int. Ed.* 2012, **51**, 10756.
17 A. Venkatesh, M. J. Ryan, A. Biswas, K. C. Boteju, A. D. Sadow and A. J. Rossini, *J. Phys. Chem. A* 2018, **122**, 5635.
18 R. Zhang, N. T. Duong, Y. Nishiyama and A. Ramamoorthy, *J. Phys. Chem. B* 2017, **121**, 5944.
19 A. Samoson, *J. Magn. Reson.* 2019, **306**, 167.
20 S. Penzel, A. Oss, M.-L. Org, A. Samoson, A. Bockmann, M. Ernst and B. Meier, *J. Biomol. NMR* 2019, **73**, 19-29.
21 M. Schledorn, A. A. Malär, A. Torosyan, S. Penzel, D. Klose, A. Oss, M.-L. Org, S. Wang, L. Lecoq, R. Cadalbert, A. Samoson, A. Böckmann and B. Meier *ChemBioChem* 2020, **21**, 2540.
22 M. M. Maricq and J. S. Waugh *J. Chem. Phys.* 1979, **70**, 3300.
23 U. Sternberg, R. Witter, I. Kuprov, J. M. Lamley, A. Oss, J. R. Lewandowski and A. Samoson, *J. Magn. Reson.* 2018, **291**, 32.
24 M. Chávez, T. Wiegand, A. A. Malär, B. H. Meier and M. Ernst, *Magn. Reson.* 2021, **2**, 499.
25 K. Xue, R. Sarkar, C. Motz, S. Asami, V. Decker, S. Wegner, Z. Tosner and B. Reif, *J. Phys. Chem. C* 2018, **122**, 16437.
26 A. Lesage, L. Duma, D. Sakellariou and L. Emsley *J. Am. Chem. Soc.* 2001, **123**, 5747.
27 H. Colaux and Y. Nishiyama *Solid State Nucl. Magn. Reson.* 2017, **87**, 104.
28 F. M. Paruzzo, B. J. Walder and L. Emsley *J. Magn. Reson.* 2019, **305**, 131.
29 P. Moutzouri, B. S. de Almeida, D. Torodii and L. Emsley, *J. Am. Chem. Soc.* 2021, **143**, 9834.
30 P. Sarder and A. Nehorai, *IEEE Signal Process Mag.* 2006, **23**, 32.
31 D. Sage, L. Donati, F. Soulez, D. Fortun, G. Schmidt, A. Seitz, R. Guiet, C. Vonesch and M. Unser, *Methods*, 2017, **115**, 28.
32 M. Makarkin and D. Bratashov, *micromachines*, 2021, **12**, 1558.
33 K. Katoh, *Curr. Med. Imaging* 2022, **20**, e020623217605.
34 K. Kazimierczuk, P. Kasprzak, P. S. Georoulia, I. Matečko-Burmann, B. M. Burrmann, L. Isaksson, E. Gustavsson, S. Westenhoff and V. Y. Orekhov, *Chem. Commun.* 2020, **56**, 14585.
35 M. Cordova, P. Moutzouri, B. S. de Almeida, D. Torodii and L. Emsley, *Angew. Chem. Int. Ed.* 2023, **62**, e202216607.
36 E. L. Hahn, *Phys. Rev.* 1950, **80**, 580.
37 https://github.com/fperras/HEAD/
38 Pokorný, V.; Touš, P.; Štejfa, V.; Růžička, K.; Rohlíček, J.; Czernek, J.; Brus, J.; Červinka, C. *Phys. Chem. Chem. Phys.* 2022, **24**, 25904.
39 B. R. Frieden and J. J. Burke, *J. Opt. Soc. Am.* 1972, **62**, 1202.
40 A. J. den Dekker and A. van den Bos, *J. Opt. Soc. Am. A* 1997, **14**, 547.
41 A. van den Bos and A. J. den Dekker, *Adv. Imaging Electron Phys.* 2001, **117**, 241.
42 M. K. Pandey, H. Kato, Y. Ishii and Y. Nishiyama *Phys. Chem. Chem. Phys.* 2016, **18**, 6209.
43 M. K. Pandey, M. Malon, A. Ramamoorthy and Y. Nishiyama *J. Magn. Reson.* 2015, **250**, 45.

